Measurement of the dijet invariant mass cross section in $p\overline{p}$ collisions at $\sqrt{s} = 1.96$ TeV

V.M. Abazov[36], B. Abbott[74], M. Abolins[63], B.S. Acharya[29], M. Adams[49], T. Adams[47], E. Aguilo[6], G.D. Alexeev[36], G. Alkhazov[40], A. Alton[62,a], G. Alverson[61], G.A. Alves[2], L.S. Ancu[35], M. Aoki[48], Y. Arnoud[14], M. Arov[58], A. Askew[47], B. Åsman[41], O. Atramentov[66], C. Avila[8], J. BackusMayes[81], F. Badaud[13], L. Bagby[48], B. Baldin[48], D.V. Bandurin[47], S. Banerjee[29], E. Barberis[61], A.-F. Barfuss[15], P. Baringer[56], J. Barreto[2], J.F. Bartlett[48], U. Bassler[18], S. Beale[6], A. Bean[56], M. Begalli[3], M. Begel[72], C. Belanger-Champagne[41], L. Bellantoni[48], J.A. Benitez[63], S.B. Beri[27], G. Bernardi[17], R. Bernhard[22], I. Bertram[42], M. Besançon[18], R. Beuselinck[43], V.A. Bezzubov[39], P.C. Bhat[48], V. Bhatnagar[27], G. Blazey[50], S. Blessing[47], K. Bloom[65], A. Boehnlein[48], D. Boline[60], T.A. Bolton[57], E.E. Boos[38], G. Borissov[42], T. Bose[60], A. Brandt[77], R. Brock[63], G. Brooijmans[69], A. Bross[48], D. Brown[19], X.B. Bu[7], D. Buchholz[51], M. Buehler[80], V. Buescher[24], V. Bunichev[38], S. Burdin[42,b], T.H. Burnett[81], C.P. Buszello[43], P. Calfayan[25], B. Calpas[15], S. Calvet[16], E. Camacho-Pérez[33], J. Cammin[70], M.A. Carrasco-Lizarraga[33], E. Carrera[47], B.C.K. Casey[48], H. Castilla-Valdez[33], S. Chakrabarti[71], D. Chakraborty[50], K.M. Chan[54], A. Chandra[79], G. Chen[56], S. Chevalier-Théry[18], D.K. Cho[76], S.W. Cho[31], S. Choi[32], B. Choudhary[28], T. Christoudias[43], S. Cihangir[48], D. Claes[65], J. Clutter[56], M. Cooke[48], W.E. Cooper[48], M. Corcoran[79], F. Couderc[18], M.-C. Cousinou[15], D. Cutts[76], M. Ćwiok[30], A. Das[45], G. Davies[43], K. De[77], S.J. de Jong[35], E. De La Cruz-Burelo[33], K. DeVaughan[65], F. Déliot[18], M. Demarteau[48], R. Demina[70], D. Denisov[48], S.P. Denisov[39], S. Desai[48], H.T. Diehl[48], M. Diesburg[48], A. Dominguez[65], T. Dorland[81], A. Dubey[28], L.V. Dudko[38], L. Duflot[16], D. Duggan[66], A. Duperrin[15], S. Dutt[27], A. Dyshkant[50], M. Eads[65], D. Edmunds[63], J. Ellison[46], V.D. Elvira[48], Y. Enari[17], S. Eno[59], H. Evans[52], A. Evdokimov[72], V.N. Evdokimov[39], G. Facini[61], A.V. Ferapontov[76], T. Ferbel[59,70], F. Fiedler[24], F. Filthaut[35], W. Fisher[63], H.E. Fisk[48], M. Fortner[50], H. Fox[42], S. Fuess[48], T. Gadfort[72], A. Garcia-Bellido[70], V. Gavrilov[37], P. Gay[13], W. Geist[19], W. Geng[15,63], D. Gerbaudo[67], C.E. Gerber[49], Y. Gershtein[66], D. Gillberg[6], G. Ginther[48,70], G. Golovanov[36], B. Gómez[8], A. Goussiou[81], P.D. Grannis[71], S. Greder[19], H. Greenlee[48], Z.D. Greenwood[58], E.M. Gregores[4], G. Grenier[20], Ph. Gris[13], J.-F. Grivaz[16], A. Grohsjean[18], S. Grünendahl[48], M.W. Grünewald[30], F. Guo[71], J. Guo[71], G. Gutierrez[48], P. Gutierrez[74], A. Haas[69,c], P. Haefner[25], S. Hagopian[47], J. Haley[61], I. Hall[63], L. Han[7], K. Harder[44], A. Harel[70], J.M. Hauptman[55], J. Hays[43], T. Hebbeker[21], D. Hedin[50], A.P. Heinson[46], U. Heintz[76], C. Hensel[23], I. Heredia-De La Cruz[33], K. Herner[62], G. Hesketh[61], M.D. Hildreth[54], R. Hirosky[80], T. Hoang[47], J.D. Hobbs[71], B. Hoeneisen[12], M. Hohlfeld[24], S. Hossain[74], P. Houben[34], Y. Hu[71], Z. Hubacek[10], N. Huske[17], V. Hynek[10], I. Iashvili[68], R. Illingworth[48], A.S. Ito[48], S. Jabeen[76], M. Jaffré[16], S. Jain[68], D. Jamin[15], R. Jesik[43], K. Johns[45], C. Johnson[69], M. Johnson[48], D. Johnston[65], A. Jonckheere[48], P. Jonsson[43], A. Juste[48,d], E. Kajfasz[15], D. Karmanov[38], P.A. Kasper[48], I. Katsanos[65], R. Kehoe[78], S. Kermiche[15], N. Khalatyan[48], A. Khanov[75], A. Kharchilava[68], Y.N. Kharzheev[36], D. Khatidze[76], M.H. Kirby[51], M. Kirsch[21], J.M. Kohli[27], A.V. Kozelov[39], J. Kraus[63], A. Kumar[68], A. Kupco[11], T. Kurča[20], V.A. Kuzmin[38], J. Kvita[9], S. Lammers[52], G. Landsberg[76], P. Lebrun[20], H.S. Lee[31], W.M. Lee[48], J. Lellouch[17], L. Li[46], Q.Z. Li[48], S.M. Lietti[5], J.K. Lim[31], D. Lincoln[48], J. Linnemann[63], V.V. Lipaev[39], R. Lipton[48], Y. Liu[7], Z. Liu[6], A. Lobodenko[40], M. Lokajicek[11], P. Love[42], H.J. Lubatti[81], R. Luna-Garcia[33,e], A.L. Lyon[48], A.K.A. Maciel[2], D. Mackin[79], R. Magaña-Villalba[33], P.K. Mal[45], S. Malik[65], V.L. Malyshev[36], Y. Maravin[57], J. Martínez-Ortega[33], R. McCarthy[71], C.L. McGivern[56], M.M. Meijer[35], A. Melnitchouk[64], L. Mendoza[8], D. Menezes[50], P.G. Mercadante[4], M. Merkin[38], A. Meyer[21], J. Meyer[23], N.K. Mondal[29], T. Moulik[56], G.S. Muanza[15], M. Mulhearn[80], E. Nagy[15], M. Naimuddin[28], M. Narain[76], R. Nayyar[28], H.A. Neal[62], J.P. Negret[8], P. Neustroev[40], H. Nilsen[22], S.F. Novaes[5], T. Nunnemann[25], G. Obrant[40], D. Onoprienko[57], J. Orduna[33], N. Osman[43], J. Osta[54], G.J. Otero y Garzón[1], M. Owen[44], M. Padilla[46], M. Pangilinan[76], N. Parashar[53], V. Parihar[76], S.-J. Park[23], S.K. Park[31], J. Parsons[69], R. Partridge[76], N. Parua[52], A. Patwa[72], B. Penning[48], M. Perfilov[38], K. Peters[44], Y. Peters[44], P. Pétroff[16], R. Piegaia[1], J. Piper[63], M.-A. Pleier[72], P.L.M. Podesta-Lerma[33,f], V.M. Podstavkov[48], M.-E. Pol[2], P. Polozov[37], A.V. Popov[39], M. Prewitt[79], D. Price[52], S. Protopopescu[72], J. Qian[62], A. Quadt[23], B. Quinn[64], M.S. Rangel[16], K. Ranjan[28], P.N. Ratoff[42], I. Razumov[39], P. Renkel[78], P. Rich[44], M. Rijssenbeek[71], I. Ripp-Baudot[19], F. Rizatdinova[75], M. Rominsky[48], C. Royon[18], P. Rubinov[48], R. Ruchti[54], G. Safronov[37], G. Sajot[14], A. Sánchez-Hernández[33], M.P. Sanders[25], B. Sanghi[48], G. Savage[48], L. Sawyer[58], T. Scanlon[43], D. Schaile[25], R.D. Schamberger[71], Y. Scheglov[40], H. Schellman[51], T. Schliephake[26], S. Schlobohm[81], C. Schwanenberger[44], R. Schwienhorst[63], J. Sekaric[56], H. Severini[74],

E. Shabalina[23], V. Shary[18], A.A. Shchukin[39], R.K. Shivpuri[28], V. Simak[10], V. Sirotenko[48], P. Skubic[74], P. Slattery[70], D. Smirnov[54], G.R. Snow[65], J. Snow[73], S. Snyder[72], S. Söldner-Rembold[44], L. Sonnenschein[21], A. Sopczak[42], M. Sosebee[77], K. Soustruznik[9], B. Spurlock[77], J. Stark[14], V. Stolin[37], D.A. Stoyanova[39], M.A. Strang[68], E. Strauss[71], M. Strauss[74], R. Ströhmer[25], D. Strom[49], L. Stutte[48], P. Svoisky[35], M. Takahashi[44], A. Tanasijczuk[1], W. Taylor[6], B. Tiller[25], M. Titov[18], V.V. Tokmenin[36], D. Tsybychev[71], B. Tuchming[18], C. Tully[67], P.M. Tuts[69], R. Unalan[63], L. Uvarov[40], S. Uvarov[40], S. Uzunyan[50], R. Van Kooten[52], W.M. van Leeuwen[34], N. Varelas[49], E.W. Varnes[45], I.A. Vasilyev[39], P. Verdier[20], L.S. Vertogradov[36], M. Verzocchi[48], M. Vesterinen[44], D. Vilanova[18], P. Vint[43], P. Vokac[10], H.D. Wahl[47], M.H.L.S. Wang[70], J. Warchol[54], G. Watts[81], M. Wayne[54], G. Weber[24], M. Weber[48,g], M. Wetstein[59], A. White[77], D. Wicke[24], M.R.J. Williams[42], G.W. Wilson[56], S.J. Wimpenny[46], M. Wobisch[58], D.R. Wood[61], T.R. Wyatt[44], Y. Xie[48], C. Xu[62], S. Yacoob[51], R. Yamada[48], W.-C. Yang[44], T. Yasuda[48], Y.A. Yatsunenko[36], Z. Ye[48], H. Yin[7], K. Yip[72], H.D. Yoo[76], S.W. Youn[48], J. Yu[77], S. Zelitch[80], T. Zhao[81], B. Zhou[62], J. Zhu[71], M. Zielinski[70], D. Zieminska[52], and L. Zivkovic[69]

(The DØ Collaboration)

[1] *Universidad de Buenos Aires, Buenos Aires, Argentina*
[2] *LAFEX, Centro Brasileiro de Pesquisas Físicas, Rio de Janeiro, Brazil*
[3] *Universidade do Estado do Rio de Janeiro, Rio de Janeiro, Brazil*
[4] *Universidade Federal do ABC, Santo André, Brazil*
[5] *Instituto de Física Teórica, Universidade Estadual Paulista, São Paulo, Brazil*
[6] *Simon Fraser University, Burnaby, British Columbia, Canada; and York University, Toronto, Ontario, Canada*
[7] *University of Science and Technology of China, Hefei, People's Republic of China*
[8] *Universidad de los Andes, Bogotá, Colombia*
[9] *Center for Particle Physics, Charles University, Faculty of Mathematics and Physics, Prague, Czech Republic*
[10] *Czech Technical University in Prague, Prague, Czech Republic*
[11] *Center for Particle Physics, Institute of Physics, Academy of Sciences of the Czech Republic, Prague, Czech Republic*
[12] *Universidad San Francisco de Quito, Quito, Ecuador*
[13] *LPC, Université Blaise Pascal, CNRS/IN2P3, Clermont, France*
[14] *LPSC, Université Joseph Fourier Grenoble 1, CNRS/IN2P3, Institut National Polytechnique de Grenoble, Grenoble, France*
[15] *CPPM, Aix-Marseille Université, CNRS/IN2P3, Marseille, France*
[16] *LAL, Université Paris-Sud, IN2P3/CNRS, Orsay, France*
[17] *LPNHE, Universités Paris VI and VII, CNRS/IN2P3, Paris, France*
[18] *CEA, Irfu, SPP, Saclay, France*
[19] *IPHC, Université de Strasbourg, CNRS/IN2P3, Strasbourg, France*
[20] *IPNL, Université Lyon 1, CNRS/IN2P3, Villeurbanne, France and Université de Lyon, Lyon, France*
[21] *III. Physikalisches Institut A, RWTH Aachen University, Aachen, Germany*
[22] *Physikalisches Institut, Universität Freiburg, Freiburg, Germany*
[23] *II. Physikalisches Institut, Georg-August-Universität Göttingen, Göttingen, Germany*
[24] *Institut für Physik, Universität Mainz, Mainz, Germany*
[25] *Ludwig-Maximilians-Universität München, München, Germany*
[26] *Fachbereich Physik, University of Wuppertal, Wuppertal, Germany*
[27] *Panjab University, Chandigarh, India*
[28] *Delhi University, Delhi, India*
[29] *Tata Institute of Fundamental Research, Mumbai, India*
[30] *University College Dublin, Dublin, Ireland*
[31] *Korea Detector Laboratory, Korea University, Seoul, Korea*
[32] *SungKyunKwan University, Suwon, Korea*
[33] *CINVESTAV, Mexico City, Mexico*
[34] *FOM-Institute NIKHEF and University of Amsterdam/NIKHEF, Amsterdam, The Netherlands*
[35] *Radboud University Nijmegen/NIKHEF, Nijmegen, The Netherlands*
[36] *Joint Institute for Nuclear Research, Dubna, Russia*
[37] *Institute for Theoretical and Experimental Physics, Moscow, Russia*
[38] *Moscow State University, Moscow, Russia*
[39] *Institute for High Energy Physics, Protvino, Russia*
[40] *Petersburg Nuclear Physics Institute, St. Petersburg, Russia*
[41] *Stockholm University, Stockholm, Sweden, and Uppsala University, Uppsala, Sweden*
[42] *Lancaster University, Lancaster LA1 4YB, United Kingdom*
[43] *Imperial College London, London SW7 2AZ, United Kingdom*

[44] *The University of Manchester, Manchester M13 9PL, United Kingdom*
[45] *University of Arizona, Tucson, Arizona 85721, USA*
[46] *University of California Riverside, Riverside, California 92521, USA*
[47] *Florida State University, Tallahassee, Florida 32306, USA*
[48] *Fermi National Accelerator Laboratory, Batavia, Illinois 60510, USA*
[49] *University of Illinois at Chicago, Chicago, Illinois 60607, USA*
[50] *Northern Illinois University, DeKalb, Illinois 60115, USA*
[51] *Northwestern University, Evanston, Illinois 60208, USA*
[52] *Indiana University, Bloomington, Indiana 47405, USA*
[53] *Purdue University Calumet, Hammond, Indiana 46323, USA*
[54] *University of Notre Dame, Notre Dame, Indiana 46556, USA*
[55] *Iowa State University, Ames, Iowa 50011, USA*
[56] *University of Kansas, Lawrence, Kansas 66045, USA*
[57] *Kansas State University, Manhattan, Kansas 66506, USA*
[58] *Louisiana Tech University, Ruston, Louisiana 71272, USA*
[59] *University of Maryland, College Park, Maryland 20742, USA*
[60] *Boston University, Boston, Massachusetts 02215, USA*
[61] *Northeastern University, Boston, Massachusetts 02115, USA*
[62] *University of Michigan, Ann Arbor, Michigan 48109, USA*
[63] *Michigan State University, East Lansing, Michigan 48824, USA*
[64] *University of Mississippi, University, Mississippi 38677, USA*
[65] *University of Nebraska, Lincoln, Nebraska 68588, USA*
[66] *Rutgers University, Piscataway, New Jersey 08855, USA*
[67] *Princeton University, Princeton, New Jersey 08544, USA*
[68] *State University of New York, Buffalo, New York 14260, USA*
[69] *Columbia University, New York, New York 10027, USA*
[70] *University of Rochester, Rochester, New York 14627, USA*
[71] *State University of New York, Stony Brook, New York 11794, USA*
[72] *Brookhaven National Laboratory, Upton, New York 11973, USA*
[73] *Langston University, Langston, Oklahoma 73050, USA*
[74] *University of Oklahoma, Norman, Oklahoma 73019, USA*
[75] *Oklahoma State University, Stillwater, Oklahoma 74078, USA*
[76] *Brown University, Providence, Rhode Island 02912, USA*
[77] *University of Texas, Arlington, Texas 76019, USA*
[78] *Southern Methodist University, Dallas, Texas 75275, USA*
[79] *Rice University, Houston, Texas 77005, USA*
[80] *University of Virginia, Charlottesville, Virginia 22901, USA and*
[81] *University of Washington, Seattle, Washington 98195, USA*

The inclusive dijet production double differential cross section as a function of the dijet invariant mass and of the largest absolute rapidity (y_{max}) of the two jets with the largest transverse momentum in an event is measured in $p\overline{p}$ collisions at $\sqrt{\mathrm{s}} = 1.96$ TeV using 0.7 fb^{-1} of data collected with the D0 detector at the Fermilab Tevatron Collider. The measurement is performed in six rapidity regions up to $|y| = 2.4$. Next-to-leading order perturbative QCD predictions are found to be in agreement with the data.

PACS numbers: 13.87.Ce, 12.38.Qk

The dominant process contributing to the total inelastic cross section in $p\overline{p}$ collisions at $\sqrt{s} = 1.96$ TeV is the production of hadronic jets. A measurement of the dijet production cross section as a function of the dijet invariant mass (M_{JJ}) can be used to test the predictions of perturbative quantum chromodynamics (QCD), to constrain parton distribution functions (PDFs) of the proton, and to look for signatures of physics not predicted by the standard model. This type of measurement is sensitive to quark compositeness, to extra spatial dimensions, and to undiscovered heavy particles that decay into two quarks [1–8]. The distribution presented in this paper is particularly sensitive to the PDF of gluons at high proton momentum fraction, a region in which the gluon distribution is weakly constrained. Previous measurements of the dijet invariant mass cross section in this energy regime restricted the rapidity of the jets to $|y| < 1.0$ [9–11] where $y = 0.5 \ln\left[(E + p_L)/(E - p_L)\right]$, E is the energy of the jet, and p_L is the component of momentum along the direction of the proton beam.

In this article, we present a measurement of the double differential dijet production cross section as a function of the dijet invariant mass and the variable $|y|_{\max}$, for $0 < |y|_{\max} < 2.4$. The dijet invariant mass is computed from the four momenta of the two jets with largest transverse momentum (p_T) with respect to the beam direction.

Both jets required to have $p_T > 40$ GeV. The variable $|y|_{\max}$ is defined as $|y|_{\max} = \max(|y_1|, |y_2|)$ where y_1 and y_2 are the rapidities of the two jets with the largest p_T. The cross section results are corrected for instrumental effects and presented at the particle level as defined in Ref. [12].

This measurement uses an integrated luminosity of approximately 0.7 fb^{-1} of data collected with the D0 detector [13] at the Fermilab Tevatron Collider in $p\overline{p}$ collisions at $\sqrt{s} = 1.96$ TeV during 2004–2005. Outgoing partons created in the scattering process hadronize to produce jets of particles that are detected in the finely segmented liquid-argon and uranium calorimeters which cover most of the solid angle. The central calorimeter (CC) covers the pseudorapidity region $|\eta|$ up to 1.1 ($\eta = -\ln[\tan(\theta/2)]$ where θ is the angle with respect to the proton beam direction) and the two end calorimeters (EC) extend the coverage up to $|\eta| < 4.2$. The intercryostat region (ICR) between the CC and EC contains scintillator-based detectors to improve the energy sampling in this region. Jets are reconstructed by clustering energy deposited in the calorimeter towers using an iterative seed-based cone jet algorithm including midpoints [14] with cone radius $\mathcal{R} = \sqrt{(\Delta y)^2 + (\Delta\phi)^2} = 0.7$, where ϕ is the azimuthal angle. The p_T of each jet is calculated using only calorimeter information and the location of the $p\overline{p}$ collision. The measurement is performed in six rapidity regions: $0 < |y|_{\max} \leq 0.4$, $0.4 < |y|_{\max} \leq 0.8$, $0.8 < |y|_{\max} \leq 1.2$, $1.2 < |y|_{\max} \leq 1.6$, $1.6 < |y|_{\max} \leq 2.0$, and $2.0 < |y|_{\max} \leq 2.4$.

Events are required to satisfy jet p_T or dijet invariant mass trigger requirements with minimum dijet invariant mass thresholds. Trigger efficiencies are studied by comparing observables in data sets collected with higher trigger thresholds to those collected using lower trigger thresholds in regions where the lower threshold trigger is 100% efficient. The trigger with the lowest threshold is determined to be 100% efficient in the region of interest by comparing it with an independent sample of muon-triggered events. For $|y|_{\max} \leq 1.6$, single jet triggers are used, while dijet invariant mass triggers are used for $|y|_{\max} > 1.6$. The measurement is only done in the kinematic regions where the trigger efficiency is $> 99\%$.

Events must satisfy data and jet quality requirements. The position of the $p\overline{p}$ interaction is reconstructed using a tracking system consisting of silicon microstrip detectors and scintillating fibers located inside a solenoidal magnetic field of approximately 2 T. The position of this primary vertex along the beam line is required to be within 50 cm of the detector center. This requirement is $\approx 93\%$ efficient. Requirements based on calorimeter shower shapes are used to remove the remaining background due to electrons, photons, and detector noise that mimic jets. The sample selection efficiency is $> 99\%$ ($> 97.5\%$ for $0.8 < |y|_{\max} < 1.6$). In order to suppress cosmic ray events, the requirements that $\not\!\!E_T/p_T^{\max} < 0.7$ for p_T of the highest p_T jet < 100 GeV and $\not\!\!E_T/p_T^{\max} < 0.5$ otherwise are applied, where $\not\!\!E_T$ is the transverse component of the vector sum of the momenta in all calorimeter cells and $p_T^{\max}$ is the transverse momentum of the jet with the maximum p_T. After all these requirements, the background is reduced to less than 0.1% in our sample.

The measured energy of each jet formed from calorimeter energy depositions is not the same as the energy of the particle jet defined as the object made of the particles entering the calorimeter. The jet four momentum is corrected, on average, to account for the energy response of the calorimeters, the energy showering in and out of the cone, and the additional energy from event pileup and multiple proton-antiproton interactions per beam crossing. The absolute jet energy calibration correction is determined from the missing transverse energy measured in γ + jet events for the region $|y| \leq 0.4$, while the rapidity dependence is derived from dijet events using a similar data driven method. Additionally, since this dijet sample has a large fraction of gluon initiated jets, corrections on the order of (2–4)% are made due to the difference in response between quark and gluon initiated jets as estimated using simulated jets produced with the PYTHIA event generator [15] that have been passed through a GEANT-based detector simulation [16]. The total jet energy correction varies between 50% and 20% for a jet p_T of 50 to 400 GeV and adjusts the measured jet energy to the energy of the particles that were measured in the calorimeter.

Bin sizes in $M_{\rm JJ}$ are chosen to be about twice the mass resolution and to have an efficiency and purity of about 50% as determined using a parameterized detector model. The efficiency is defined as the ratio of Monte Carlo events generated and reconstructed to those generated in a $M_{\rm JJ}$ bin, and purity is defined as the ratio of Monte Carlo events generated and reconstructed in a $M_{\rm JJ}$ bin to all events reconstructed in that bin. The detector model used is a fast simulation of the D0 detector based on parameterizations including energy and position resolutions obtained either from the data or from a detailed simulation of the D0 detector using GEANT. This detector model uses events generated by PYTHIA (using the settings of Tune QW [17] and MSTW2008LO PDFs [18]) that have been reweighted to match measured dijet invariant mass and rapidity distributions in the data. This reweighting assumes a smooth underlying distribution, which does not include resonances. After this tuning, other spectra fundamental to this measurement, such as the jet p_T distributions, show good agreement between the data and simulation. Because the underlying dijet cross sections are steeply falling, the measured dijet invariant mass distributions are systematically shifted to higher invariant mass values due to jet p_T resolution. The jet p_T resolution is measured in data using momentum conservation in the transverse plane for events with exactly two jets, and is found to be approximately 13%

(7%) at $p_T \approx 50$ (400) GeV in the CC and EC, and 16% (11%) at $p_T \approx 50$ (400) GeV in the ICR. The bin-to-bin migrations due to experimental resolution are determined using the parametrized detector model. To minimize migrations between $M_{\rm JJ}$ bins due to resolution effects, we use the simulation to obtain a rescaling function in $M_{\rm JJ}$ that optimizes the correlation between the reconstructed and true values. The total experimental corrections to the data are less than $\pm 2\%$ across the whole dijet invariant mass range for $|y|_{\rm max} < 0.8$, vary from 0.5% at $M_{\rm JJ} = 0.4$ TeV to 22% at 1.2 TeV for $0.8 < |y|_{\rm max} < 1.6$, and from 1% at $M_{\rm JJ} = 0.4$ TeV to 11% at 1.3 TeV for $1.6 < |y|_{\rm max} < 2.4$.

We compute the doubly differential dijet cross section as a function of dijet invariant mass and $|y|_{\rm max}$ corrected for all selection efficiencies and migrations due to resolution, and for the energies of unreconstructed muons and neutrinos associated with the jet. The result is plotted in all six rapidity regions in Fig. 1 and tabulated in Tables I through VI. The quoted central value of $M_{\rm JJ}$ in each bin is the location where the differential cross section has the same value as the bin average [19].

The systematic uncertainties on the cross section are dominated by the uncertainties in the jet energy calibration, which range from 6% to 22% in the CC, 8% to 30% in the ICR, and 15% to 45% in the EC region. The second largest systematic uncertainty comes from the p_T resolution uncertainty, which ranges between 2% and 10% in all regions. The luminosity determination has an uncertainty of 6.1% which is completely correlated across all bins. The systematic uncertainties on the jet identification efficiency corrections, corrections due to misvertexing and angular resolutions, and Monte Carlo reweighting are calculated using the parameterized model of the detector and affect the measured cross section by less than 2% in all regions.

The data are compared to the next-to-leading order (NLO) prediction computed using fastNLO [20] based on NLOJET++ [21, 22] for MSTW2008NLO PDFs with $\alpha_s(M_Z) = 0.120$. The NLO prediction is corrected for hadronization and underlying event effects using corrections which range between -10% and $+23\%$ depending on the mass in all rapidity regions. The correction factors are obtained by turning these effects on and off individually in PYTHIA. The uncertainty due to the non-perturbative corrections is estimated as 50% of the individual corrections, with the uncertainty determined by adding the individual contributions in quadrature. The renormalization and factorization scales are set to $\mu_R = \mu_F = p_T = (p_{T1} + p_{T2})/2$ where p_{T1} and p_{T2} are the p_T of the two highest p_T jets. The effect of varying these scales simultaneously from $\mu = p_T/2$ to $\mu = 2p_T$ is shown in Fig. 2 where the ratio of data to theory is plotted.

The experimental uncertainties are similar in size to both the PDF and the scale uncertainties, suggesting that the measurement will constrain theoretical models. We are quoting PDF uncertainties corresponding to a 90% C.L. The total uncertainties are smaller than those of earlier measurements at this same center-of-mass energy [11]. In addition to comparing the D0 measurement to the theoretical predictions using MSTW2008NLO PDFs, we also compare to the theoretical predictions using CTEQ6.6 PDFs [23]. The difference in the cross section due to the choice of PDFs is (40–60)% at the highest mass. Although the MSTW2008NLO PDFs are favored, it is important to note that their determination included a measurement of the D0 inclusive jet production cross section [24] which is based on the same dataset as the present measurement. In addition, these PDFs exclude Tevatron data taken before 2000, while the CTEQ6.6 PDFs include that data and do not include Tevatron data taken after 2000.

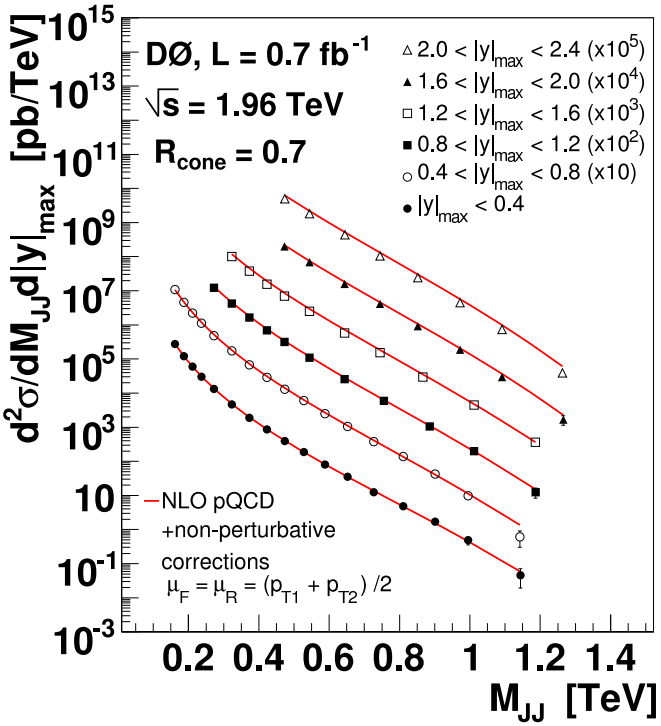

FIG. 1: (color online) The dijet production cross section as a function of invariant mass in intervals of $|y|_{\rm max}$ compared to NLO predictions that include non-perturbative corrections. Uncertainties shown are statistical only.

In summary, we have presented a new measurement of the dijet production cross section as a function of the dijet invariant mass and of the largest rapidity of the two highest p_T jets that extends the rapidity range beyond previous measurements, with systematic uncertainties that are significantly smaller. The data are described by NLO QCD predictions using MSTW2008NLO PDFs in all rapidity regions, and are not well described by CTEQ6.6 PDFs, particularly at high rapidities.

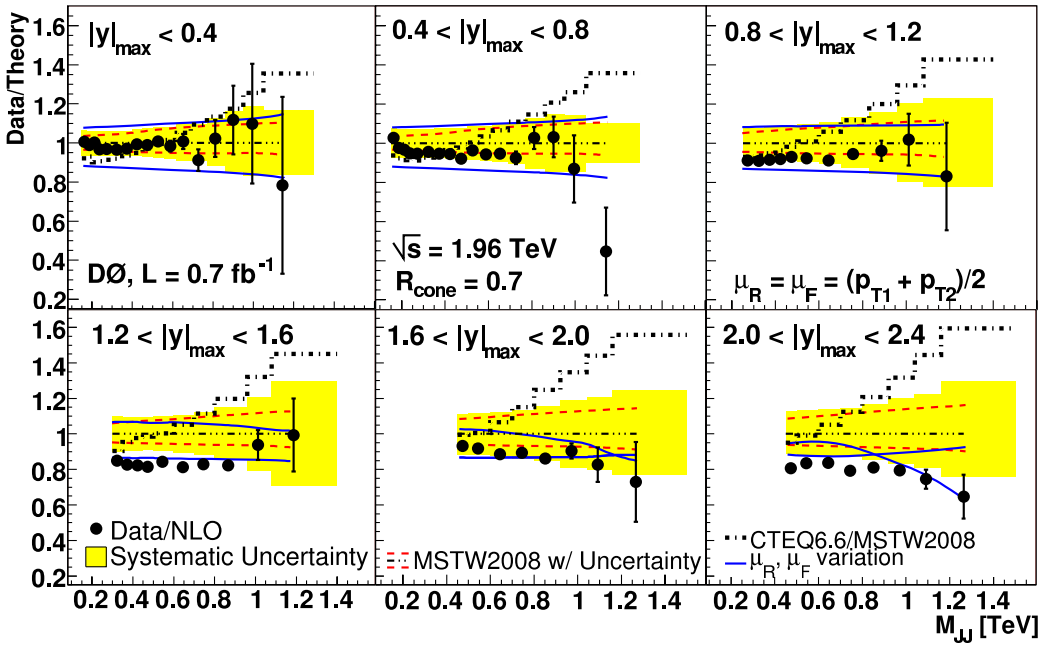

FIG. 2: (color online) Ratio of data over theoretical expectation using MSTW2008NLO PDFs in all six $|y|_{\max}$ bins. The measurement systematic uncertainty is shown as a shaded band. There is an additional fully correlated uncertainty of 6.1% due to the integrated luminosity determination which is not shown in the plots. The legend for all six plots shown is spread out over the three bottom plots with other relevant information in the top three plots.

Mass range TeV	Central value TeV	Measured Cross Section pb/TeV	Systematic uncertainty %	Statistical uncertainty %	Theory Cross Section pb/TeV	Non-perturbative corrections Hadronization	Underlying event	Total
0.150–0.175	0.162	2.74×10^{5}	+7.3,−6.6	1.6	2.72×10^{5}	0.928	1.156	1.074
0.175–0.200	0.187	1.22×10^{5}	+7.3,−6.6	2.4	1.22×10^{5}	0.935	1.137	1.064
0.200–0.225	0.212	6.00×10^{4}	+7.3,−6.6	1.0	5.93×10^{4}	0.941	1.123	1.056
0.225–0.250	0.237	3.02×10^{4}	+7.3,−6.6	1.5	3.11×10^{4}	0.945	1.112	1.050
0.250–0.300	0.272	1.32×10^{4}	+7.3,−6.6	0.8	1.36×10^{4}	0.950	1.099	1.044
0.300–0.350	0.323	4.69×10^{3}	+7.5,−6.8	1.3	4.86×10^{3}	0.955	1.087	1.037
0.350–0.400	0.373	1.90×10^{3}	+7.3,−6.7	0.8	1.96×10^{3}	0.959	1.078	1.032
0.400–0.450	0.423	8.48×10^{2}	+7.4,−6.8	1.1	8.61×10^{2}	0.961	1.071	1.029
0.450–0.500	0.473	3.93×10^{2}	+7.6,−7.1	1.4	4.01×10^{2}	0.963	1.066	1.026
0.500–0.560	0.528	1.84×10^{2}	+7.9,−7.4	1.9	1.85×10^{2}	0.965	1.061	1.024
0.560–0.620	0.588	7.93×10^{1}	+8.3,−8.0	2.9	8.17×10^{1}	0.967	1.057	1.021
0.620–0.690	0.652	3.50×10^{1}	+9.1,−8.8	4.0	3.52×10^{1}	0.968	1.054	1.020
0.690–0.770	0.727	1.23×10^{1}	+10.4,−10.0	6.4	1.37×10^{1}	0.969	1.051	1.018
0.770–0.860	0.811	4.83×10^{0}	+12.1,−11.7	9.8	4.76×10^{0}	0.970	1.048	1.017
0.860–0.950	0.901	1.69×10^{0}	+14.3,−13.7	15.8	1.52×10^{0}	0.971	1.046	1.015
0.950–1.050	0.995	4.95×10^{-1}	+16.7,−15.8	31.6	4.49×10^{-1}	0.972	1.044	1.014
1.050–1.300	1.144	4.56×10^{-2}	+22.1,−20.0	57.7	5.82×10^{-2}	0.973	1.042	1.013

TABLE I: Dijet double differential cross section, $d^2\sigma/dMd|y|_{\max}$, for $|y|_{\max} \leq 0.4$, compared to theoretical predictions with non-perturbative corrections. There is an additional fully correlated uncertainty of 6.1% due to the integrated luminosity determination which is not shown in the table.

We thank the staffs at Fermilab and collaborating institutions, and acknowledge support from the DOE and NSF (USA); CEA and CNRS/IN2P3 (France); FASI, Rosatom and RFBR (Russia); CNPq, FAPERJ, FAPESP and FUNDUNESP (Brazil); DAE and DST (India); Colciencias (Colombia); CONACyT (Mexico); KRF and KOSEF (Korea); CONICET and UBACyT (Argentina); FOM (The Netherlands); STFC and the Royal Society (United Kingdom); MSMT and GACR (Czech Republic); CRC Program and NSERC (Canada); BMBF and DFG (Germany); SFI (Ireland); The Swedish Research Council (Sweden); and CAS and CNSF (China).

Mass range TeV	Central value TeV	Measured Cross Section pb/TeV	Systematic uncertainty %	Statistical uncertainty %	Theory Cross Section pb/TeV	Non-perturbative corrections Hadron-ization	Underlying event	Total
0.150–0.175	0.162	1.08×10^{6}	+7.4,−7.4	0.8	1.06×10^{6}	0.945	1.128	1.065
0.175–0.200	0.187	4.67×10^{5}	+7.5,−7.4	1.2	4.68×10^{5}	0.949	1.113	1.056
0.200–0.225	0.212	2.24×10^{5}	+7.5,−7.5	0.5	2.28×10^{5}	0.954	1.098	1.047
0.225–0.250	0.237	1.14×10^{5}	+7.6,−7.5	0.7	1.19×10^{5}	0.957	1.088	1.040
0.250–0.300	0.272	4.91×10^{4}	+7.9,−7.8	0.4	5.14×10^{4}	0.959	1.080	1.036
0.300–0.350	0.323	1.74×10^{4}	+7.6,−7.6	0.7	1.81×10^{4}	0.961	1.073	1.032
0.350–0.400	0.373	6.77×10^{3}	+7.9,−7.7	0.4	7.16×10^{3}	0.963	1.068	1.028
0.400–0.450	0.423	2.89×10^{3}	+8.0,−7.9	0.6	3.07×10^{3}	0.964	1.063	1.026
0.450–0.500	0.473	1.28×10^{3}	+8.3,−8.2	0.8	1.40×10^{3}	0.965	1.059	1.023
0.500–0.560	0.528	5.97×10^{2}	+8.7,−8.6	1.0	6.25×10^{2}	0.966	1.056	1.021
0.560–0.620	0.589	2.50×10^{2}	+9.4,−9.2	1.6	2.68×10^{2}	0.968	1.053	1.019
0.620–0.690	0.652	1.04×10^{2}	+10.3,−10.1	2.3	1.11×10^{2}	0.968	1.050	1.017
0.690–0.770	0.726	3.78×10^{1}	+11.7,−11.3	3.6	4.12×10^{1}	0.969	1.048	1.016
0.770–0.860	0.811	1.38×10^{1}	+13.5,−13.0	5.6	1.35×10^{1}	0.970	1.045	1.014
0.860–0.950	0.901	4.20×10^{0}	+15.7, −14.9	10.7	4.07×10^{0}	0.971	1.041	1.012
0.950–1.050	0.994	9.90×10^{-1}	+18.4,−17.0	20.4	1.13×10^{0}	0.971	1.040	1.011
1.050–1.300	1.142	6.08×10^{-2}	+23.5,−20.9	50.0	1.36×10^{-1}	0.972	1.040	1.011

TABLE II: Dijet double differential cross section, $d^2\sigma/dMd|y|_{\max}$, for $0.4 < |y|_{\max} < 0.8$, compared to theoretical predictions with non-perturbative corrections. There is an additional fully correlated uncertainty of 6.1% due to the integrated luminosity determination which is not shown in the table.

Mass range TeV	Central value TeV	Measured Cross Section pb/TeV	Systematic uncertainty %	Statistical uncertainty %	Theory Cross Section pb/TeV	Non-perturbative corrections Hadron-ization	Underlying event	Total
0.250–0.300	0.272	1.21×10^{5}	+10.3,−10.0	0.5	1.33×10^{5}	0.946	1.111	1.067
0.300–0.350	0.323	4.18×10^{4}	+9.7,−9.5	0.9	4.62×10^{4}	0.950	1.101	1.058
0.350–0.400	0.373	1.63×10^{4}	+9.4,−9.1	1.4	1.80×10^{4}	0.953	1.093	1.052
0.400–0.450	0.423	6.86×10^{3}	+9.3,−9.0	1.0	7.55×10^{3}	0.955	1.086	1.048
0.450– 0.500	0.473	3.10×10^{3}	+9.3,−9.0	1.6	3.38×10^{3}	0.957	1.079	1.042
0.500–0.600	0.544	1.07×10^{3}	+9.6,−9.3	0.7	1.17×10^{3}	0.960	1.073	1.037
0.600–0.700	0.644	2.57×10^{2}	+10.6,−10.4	1.5	2.84×10^{2}	0.961	1.067	1.033
0.700–0.830	0.756	5.95×10^{1}	+12.7,−12.6	2.2	6.30×10^{1}	0.963	1.063	1.030
0.830–0.960	0.886	1.08×10^{1}	+16.4,−16.0	5.3	1.10×10^{1}	0.964	1.061	1.023
0.960–1.080	1.012	2.10×10^{0}	+20.6,−19.7	12.5	1.95×10^{0}	0.965	1.057	1.025
1.080–1.400	1.186	1.43×10^{-1}	+28.5,−24.5	28.9	1.50×10^{-1}	0.966	1.054	1.022

TABLE III: Dijet double differential cross section, $d^2\sigma/dMd|y|_{\max}$, for $0.8 < |y|_{\max} \leq 1.2$, compared to theoretical predictions with non-perturbative corrections. There is an additional fully correlated uncertainty of 6.1% due to the integrated luminosity determination which is not shown in the table.

Mass range TeV	Central value TeV	Measured Cross Section pb/TeV	Systematic uncertainty %	Statistical uncertainty %	Theory Cross Section pb/TeV	Non-perturbative corrections Hadron-ization	Underlying event	Total
0.300–0.350	0.323	1.00×10^{5}	+10.7,−10.4	0.6	1.18×10^{5}	0.950	1.144	1.081
0.350–0.400	0.373	3.79×10^{4}	+10.4,−10.1	0.9	4.59×10^{4}	0.951	1.134	1.075
0.400–0.450	0.423	1.61×10^{4}	+10.4,−9.9	1.4	1.91×10^{4}	0.952	1.127	1.069
0.450–0.500	0.473	7.11×10^{3}	+10.7,−10.0	2.1	8.59×10^{3}	0.954	1.118	1.064
0.500–0.600	0.544	2.54×10^{3}	+11.3,−10.4	1.2	2.97×10^{3}	0.955	1.110	1.058
0.600–0.700	0.644	5.94×10^{2}	+12.3,−11.7	0.9	7.15×10^{2}	0.956	1.104	1.054
0.700–0.800	0.744	1.58×10^{2}	+14.1,−13.4	1.8	1.84×10^{2}	0.956	1.099	1.051
0.800–0.960	0.866	3.16×10^{1}	+17.8,−16.8	2.8	3.57×10^{1}	0.957	1.096	1.048
0.960–1.080	1.012	5.08×10^{0}	+22.7,−21.4	7.9	4.78×10^{0}	0.958	1.092	1.045
1.080–1.400	1.186	4.77×10^{-1}	+29.5,−27.9	15.8	3.67×10^{-1}	0.958	1.088	1.042

TABLE IV: Dijet double differential cross section, $d^2\sigma/dMd|y|_{\max}$, for $1.2 < |y|_{\max} \leq 1.6$, compared to theoretical predictions with non-perturbative corrections. There is an additional fully correlated uncertainty of 6.1% due to the integrated luminosity determination which is not shown in the table.

[a] Visitor from Augustana College, Sioux Falls, SD, USA.

[b] Visitor from The University of Liverpool, Liverpool, UK.

Mass range TeV	Central value TeV	Measured Cross Section pb/TeV	Systematic uncertainty %	Statistical uncertainty %	Theory Cross Section pb/TeV	Non-perturbative corrections Hadron-ization	Underlying event	Total
0.450–0.500	0.473	2.01×10^{4}	+12.0−13.5	1.0	2.16×10^{4}	0.939	1.156	1.037
0.500–0.600	0.544	6.88×10^{3}	+13.8,−14.6	1.2	7.49×10^{3}	0.940	1.145	1.033
0.600–0.700	0.644	1.58×10^{3}	+16.3,−17.3	2.5	1.80×10^{3}	0.940	1.137	1.030
0.700–0.800	0.744	4.10×10^{2}	+19.9,−18.7	1.1	4.59×10^{2}	0.940	1.130	1.028
0.800–0.920	0.852	9.30×10^{1}	+21.1,−17.0	2.0	1.07×10^{2}	0.940	1.124	1.026
0.920–1.040	0.972	1.93×10^{1}	+27.1,−20.3	4.5	2.07×10^{1}	0.941	1.118	1.024
1.040–1.160	1.092	3.15×10^{0}	+32.5,−24.3	11.0	3.60×10^{0}	0.941	1.112	1.022
1.160–1.500	1.266	1.92×10^{-1}	+36.3,−33.4	25.0	2.28×10^{-1}	0.941	1.109	1.021

TABLE V: Dijet double differential cross section, $d^2\sigma/dMd|y|_{\max}$, for $1.6 < |y|_{\max} \leq 2.0$, compared to theoretical predictions with non-perturbative corrections. There is an additional fully correlated uncertainty of 6.1% due to the integrated luminosity determination which is not shown in the table.

Mass range TeV	Central value TeV	Measured Cross Section pb/TeV	Systematic uncertainty %	Statistical uncertainty %	Theory Cross Section pb/TeV	Non-perturbative corrections Hadron-ization	Underlying event	Total
0.450–0.500	0.473	4.95×10^{4}	+16.1,−13.7	0.6	6.15×10^{4}	0.901	1.230	1.151
0.500–0.600	0.544	1.81×10^{4}	+16.2,−14.1	0.7	2.17×10^{4}	0.902	1.222	1.138
0.600–0.700	0.644	4.36×10^{3}	+16.5,−15.2	1.5	5.25×10^{3}	0.902	1.215	1.127
0.700–0.800	0.744	1.02×10^{3}	+17.4,−17.0	0.7	1.31×10^{3}	0.903	1.209	1.119
0.800–0.920	0.852	2.37×10^{2}	+20.0,−19.9	1.3	2.99×10^{2}	0.903	1.205	1.113
0.920–1.040	0.972	4.43×10^{1}	+24.8,−23.9	2.9	5.68×10^{1}	0.903	1.200	1.105
1.040–1.160	1.091	7.25×10^{0}	+33.0,−28.0	7.0	9.88×10^{0}	0.904	1.195	1.098
1.160–1.500	1.263	4.12×10^{-1}	+46.1,−33.8	16.4	6.10×10^{-1}	0.904	1.193	1.095

TABLE VI: Dijet double differential cross section, $d^2\sigma/dMd|y|_{\max}$, for $2.0 < |y|_{\max} \leq 2.4$, compared to theoretical predictions with non-perturbative corrections. There is an additional fully correlated uncertainty of 6.1% due to the integrated luminosity determination which is not shown in the table.

[c] Visitor from SLAC, Menlo Park, CA, USA.
[d] Visitor from ICREA/IFAE, Barcelona, Spain.
[e] Visitor from Centro de Investigacion en Computacion - IPN, Mexico City, Mexico.
[f] Visitor from ECFM, Universidad Autonoma de Sinaloa, Culiacán, Mexico.
[g] Visitor from Universität Bern, Bern, Switzerland.

[1] E. Eichten, K. Lane, M.E. Peskin, Phys. Rev. Lett. 50 (1983) 811.
[2] E. Eichten, I. Hinchcliffe, K. Lane, C. Quigg, Rev. Mod. Phys. 56 (1984) 579; Addendum *ibid.* 58 (1986) 1065.
[3] K. Lane, arXiv:hep-ph/9605257.
[4] N. Arkani-Hamed, S. Dimopoulos, G. R. Dvali, Phys. Lett. B 429 (1998) 263.
[5] D. Atwood, S. Bar-Shalom, A. Soni, Phys. Rev. D 62 (2000) 056008.
[6] K. R. Dienes, E. Dudas, T. Gherghetta, Nucl. Phys. B 537 (1999) 47.
[7] A. Pomarol, M. Quiros, Phys. Lett. B 438 (1998) 255.
[8] K. Cheung, G. Landsberg, Phys. Rev. D 65 (2002) 076003.
[9] B. Abbott et al. (D0 Collaboration), Phys. Rev. D 64 (2001) 032003.
[10] B. Abbott et al. (D0 Collaboration), Phys. Rev. Lett. 82 (1999) 2457.
[11] T. Aaltonen et al. (CDF Collaboration), Phys. Rev. D 29 (2009) 112002.
[12] C. Buttar et al., arXiv:hep-ph/0803.0678 [hep-ph].
[13] V.M. Abazov et al. (D0 Collaboration), Nucl. Instrum. Methods Phys. Res. A 565 (2006) 463.
[14] G.C. Blazey et al., in *Proceedings of the Workshop: QCD and Weak Boson Physics in Run II,* edited by U. Baur, R.K. Ellis, D. Zeppenfeld, Fermilab-Pub-00/297 (2000).
[15] T. Sjöstrand et al., Comput. Phys. Commun. 135 (2001) 238.
[16] R. Brun, F. Carminati, CERN Program Library Long Writeup Report No. W5013, 1993 (unpublished).
[17] M. G. Albrow et al. [TeV4LHC QCD Working Group], arXiv:hep-ph/0610012.
[18] A.D. Martin, W.J. Stirling, R.S Thorne, G. Watt, Eur. Phys. J. C 63 (2009) 189.
[19] G.D. Lafferty, T.R. Wyatt, Nucl. Instrum. Meth. A 355 (1995) 541.
[20] T. Kluge, K. Rabbertz, M. Wobisch, arXiv:hep-ph/0609285.
[21] Z. Nagy, Phys. Rev. D 68 (2003) 094002.
[22] Z. Nagy, Phys. Rev. Lett. 88 (2002) 122003.
[23] P.M. Nadolsky et al., Phys. Rev. D 78 (2008) 013004.
[24] V.M. Abazov et al., Phys. Rev. Lett. 101 (2008) 062001.